Collagen Biocomposites Derived from Fish Waste: Doped and Cross-Linked with Functionalized Fe₃O₄ Nanoparticles and Their Comparative Studies with a Green Approach

Abhishek Mandal,* Ezhumalai Dhineshkumar, and Eagambaram Murugan*

ACCESS | Metrics & More | Article Recommendations

ABSTRACT: Collagen-based nanobiocomposites can reabsorb and are biode-gradable. These properties are effectively controlled by the number of cross-links. This study demonstrates an effortless and proficient approach for the functionalization of Fe₃O₄ NPs for cross-linking collagen obtained from biowaste, viz., fish scales of *Lates Calcarifer*, a marine origin. The size of Fe₃O₄ NPs (10−40 nm) was confirmed using particle size analysis. The physico-chemical properties of the aminosilane-coated Fe₃O₄ NPs cross-linked via succinylated collagen (FFCSC) were characterized using different analytical techniques and compared with succinylated collagen doped with Fe₃O₄ NPs (FDSC). Thermogravimetric analysis indicates cross-linked product FFCSC to be more stable than the FDSC. Also, the antibacterial effect was more pronounced for FFCSC than for FDSC nano-biocomposites. FFCSC exhibited improved mechanical properties which are essential for materials used for wound dressing purposes. Moreover, the cell viability of fibroblasts (3T3-L1) and their morphology studied by SEM and fluorescence microscopy showed biocompatibility of both FDSC and FFCSC. Thus, the current investigation, involves a waste to wealth approach where the collagen-based nanobiocomposites present an easy way to recycle the biowaste to value-added products using simple and clean methods, which are suitable for use in biomedical and environmental applications.
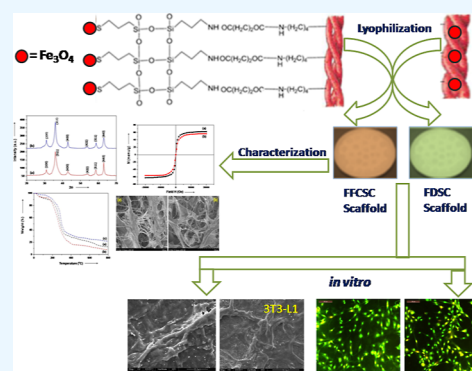
1. INTRODUCTION

Collagen is a structural protein and a biopolymer and considered as a versatile biomaterial due to its better biological properties, which lead to its profound use in biomedical applications.[1] However, there are certain drawbacks of denaturation at temperatures above 37 °C and its inability to dissolve in neutral pH buffers that limit its application in tissue engineering and regenerative medicine.[2,3] Specifically, collagen extracted from bovine sources is the most common but increased reports on transmissible diseases in collagen-based products have led to the search for an alternate source.[4−6] Moreover, researchers have focused on the sustainable pathways to perform the conversion of bio-waste to value-added products such as catalysts useful for various industrial applications.[7−12] Fish scales, which are non-edible bio-waste, produce an obnoxious smell when kept aside for a longer duration and cause environmental pollution.[13,14] However, these fish processing wastes can be utilized for various industrial applications.[15−19] Additionally, collagen can be derived from fish scales, which become an excellent alternative to the bovine source and are free from transmissible diseases in the developed products.[20,21] Despite these benefits, the collagen extracted from fish scales, especially from marine origin has a low denaturation temperature. Also, the high rate

of biodegradation and low mechanical stability of collagen are the major problems to be solved for its application.[22−24] A simple procedure usually adopted to overcome the above-mentioned problem is to crosslink collagen, which reduces the biodegradation and also enhances the mechanical stability of collagen in the native state. However, this procedure is unsuitable for several in vivo based applications.[25,26] After this study, collagen-based materials crosslinked via succinylation have been reported in the recent past.[27,28] In this study, it is established that succinic anhydride restricts the breaking of lysyl peptide bonds of trypsin, and hence, one positive charge is substituted by two negative units of charge, which leads to polyanionic collagen at physiological pH.[26]
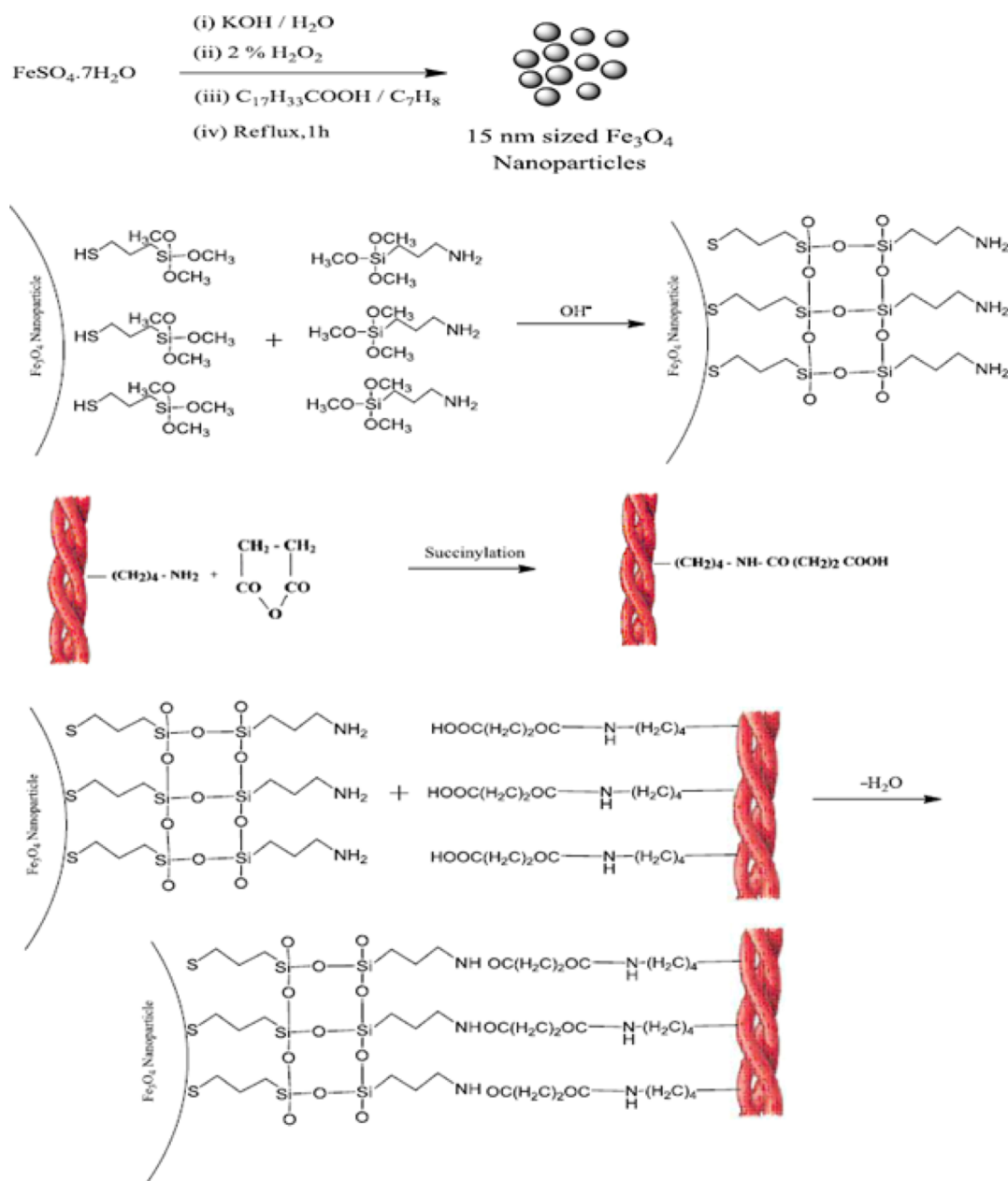
It is also essential to highlight here that the magnetite nanoparticles (Fe₃O₄ NPs) are well known to exhibit properties such as nano-size and superparamagnetism, which have been extensively used in various pharmaceutical and

Scheme 1. Synthesis of Amine-Functionalized Fe₃O₄ Nanoparticles Crosslinked with Succinylated Collagen

medical applications.[29−31] Though Fe₃O₄ NPs are used for numerous biological purposes mainly in drug delivery,[32,33] cell seeding process in scaffolds,[34−36] cell tracking,[37] hyperthermia,[38] and as MRI contrast agent for the treatment of cancers,[39] the low solubility and hydrophobic surfaces result in their aggregation via dipole−dipole attractions between particles.[40−42] Thus, surface coating is necessary, which enables the homogeneous dispersion by the formation of hydrophilic surfaces that provide stability to the Fe₃O₄ NPs.[43] Hence, surface modifications of NPs and their interaction with various biodegradable polymers, which are also biocompatible have been the subject of interest and thus are widely investigated.[44,45] The capping of Fe₃O₄ NPs with silanes has been investigated in the recent past.[46−51] However, very few studies on the interaction of functionalized Fe₃O₄ NPs with collagen is documented. Additionally, so far, no study on the comparison between collagen nanobiocomposites doped with Fe₃O₄ NPs

and cross-linked with functionalized Fe₃O₄ NPs has been reported previously. Consequently, motive of the work is to design, characterize, and conduct a comparative study of the collagen nanobiocomposites derived from biowaste, i.e., fish scales of marine origin, viz., *Lates Calcarifer*, which are doped with Fe₃O₄ NPs and cross-linked with functionalized Fe₃O₄ NPs for various biological and environmental applications. A simple and efficient approach to cross-link aminosilane functionalized Fe₃O₄ NPs with collagen is described in this present investigation. Multiple amine groups on the Fe₃O₄ NPs surfaces enable links up with collagen. The peptide bonds formation due to −COOH groups present in collagen is increased when succinylation is performed. Moreover, the stability, physico-chemical properties, and biocompatibility of these fabricated nanobiocomposites were investigated.

2. MATERIALS AND METHODS

2.1. Materials. The chemicals as well as reagents for this investigation were procured from Sigma-Aldrich (AG). Also, deionized water was utilized for the complete study.

2.2. Instrumentation. Fourier transform-infrared (FT-IR) analysis was conducted on a PerkinElmer Spectrum 2000 instrument. Pellets were prepared by mixing 2 mg of sample with KBr (1:5) via a hydraulic press and spectra recorded from 400 to 4000 cm^{-1} with a resolution of 2 cm^{-1}. Circular dichroism (CD) studies for the confirmation of collagen were conducted on a spectropolarimeter (JASCO J-715 model). Thermal analyses (DSC and TGA) of the nanobiocomposites were assessed with a PerkinElmer Model. The thermograms for samples placed in aluminum pans heated at a rate of 10 °C/min from 30 to 300 °C in a N$_2$ atmosphere were recorded. The samples were sputter coated with gold to study the surface morphology using scanning electron microscopy (SEM), Philips XL-30. Also, the morphologies of Fe$_3$O$_4$ doped on succinylated collagen (FDSC) and functionalization Fe$_3$O$_4$ cross-linked to succinylated collagen (FFCSC) were studied via a tunneling electron microscope (model: Jem-2100). Malvern-based Zetasizer model no. 3000 HSA was used to gather vital information on zeta potential and particle size distribution. The paramagnetic effect of the nanobiocomposite was determined from the vibration sample magnetometer (VSM 7300-model). The mechanical characteristics of NBCs were obtained using SATRA, UK, model no. TM-43 at 25 °C. The prepared NBCs in the form of dumbbells with 16 mm were immersed in distilled water for 30 min and the tensile force were applied at an extension rate of 10 mm/min. Pneumatic grips subjected to 40 psi pressure were used to clamp the sample specimen and the tensile strengths of the NBCs were determined.

2.3. Synthesis and Functionalization of Fe$_3$O$_4$ NPs. Fe$_3$O$_4$ NPs were prepared using two-phase water/toluene system that also contained oleic acid.[52] Functionalization of Fe$_3$O$_4$ NPs was achieved by two-step silanization processes at 60 ± 3 °C.[53] 2 mL of 0.1 M (3-mercaptopropyl)-trimethoxysilane and (3-aminopropyl) trimethoxysilane (APTMS) were added to 2 mL of 0.1 M Fe$_3$O$_4$ NP dispersion. The contents were heated at 60 ± 3 °C, and the obtained precipitate separated and repeated methanol washing was carried out. To the precipitate was added toluene and tetra butyl ammonium hydroxide and contents were heated at 60 ± 3 °C for 2 h. The solid precipitate was washed with toluene to remove the excess silane and bases.

2.4. Fe$_3$O$_4$ NPs Cross-Linking to Collagen via Succinylation. The aminosilane-functionalized Fe$_3$O$_4$ NPs were cross-linked with succinylated collagen (SC). Collagen was isolated from the scales of marine fish, *Lates Calcarifer*.[14] The method of succinylation of collagen was reported earlier.[5] 10 g of collagen added in 4 L water and pH 2.5 adjusted by dil. HCl. To the solubilized collagen, NaOH solution was added to obtain pH 9. Then, succinic anhydride solution (2%) was added to the contents and the SC precipitation was done at pH 4 using dilute HCl. The entire process was conducted in ice-cold conditions. The yield and purity of acid solubilized collagen were found to be 0.58% (based on dry weight) and 20%, respectively. For the preparation of nanobiocomposites, a homogenizer was used for the mixing of the functionalized Fe$_3$O$_4$ NPs (60 μL, 0.1 M) with SC (1% soln.), followed by the lyophilization process carried out at −80 °C. To further stabilize these nanobiocomposites, 1-ethyl-3-(3-dimethylaminopropyl)carbodiimidehydrochloride (EDC) and *N*-hydroy succinimide (NHS) in 50 mM 4-morpholine ethane sulfonic acid in 40% ethanol (MES soln) were added. The soln. pH was adjusted to 5 with the help of 0.1 M NaOH soln. Also, nanobiocomposites of SC doped with 60 μL of 0.1 M Fe$_3$O$_4$ NPs (FDSC) were prepared. The preparation of FFCSC nanobiocomposites is depicted in Scheme 1.

Ninhydrin assay, a method that provides the amount of free amines, was employed in the functionalized SC.[54−56] To explain, 4% (w/v) of ninhydrin in 100 mL of ethylene glycol monoethyl ether was added to a mixture of 100 mM citric acid and 0.16% (w/v) SnCl$_2$. The contents were thoroughly mixed by maintaining pH 5 through the addition of 5 M NaOH. The nanobiocomposites (50 mg) were weighed and immersed in the contents and then further incubated at 80 °C for 45 min. Subsequently, 300 μL of isopropanol was added to the nanobiocomposites, which lead to the purple color formation. The absorbance was recorded at 570 nm.

2.5. Biodegradability Assay. For the biodegradability experiment of the Fe$_3$O$_4$ NPs in collagen-based nanobiocomposites (FDSC and FFCSC), the procedure of Kesava Reddy and Enwemeka[57] was used, i.e., 20 mg of nanobiocomposites was incubated at 40 °C for 120 h after treatments with enzyme buffer (150 μL) and collagenase enzyme (500 μL) procured from Sigma-Aldrich. After every 12 h, the released amount of the hydroxyproline was determined via the method used by Woessner.[58]

2.6. Antibacterial Studies. For the nanobiocomposites, minimum inhibitory concentration (MIC) was carried out on two different bacterial cultures: *Staphylococcus aureus* (ATCC 25923), which is Gram-positive, and *Escherichia coli* (ATCC 25922), a Gram-negative strain, using CLSI/NCCLS methods.[59] The experiment was carried out in triplicates and values are reported as mean ± SD.

2.7. Biocompatibility and Cell Culture Studies. The compatibility of the nanobiocomposites was determined using the procedure mentioned in Mandal et al.[24] The procedure for cell culture of mice fibroblasts (3T3-L1) were carried out by following the protocol used in Mandal et al.[24,60]

2.8. Viability Study on Collagen Nanobiocomposites. The viability for fibroblast cells on collagen nanobiocomposites, viz., FDSC and FFCSC, was carried out via the methylthiazol tetrazolium (MTT) assay. The seeding of the 3T3-L1 cells was allowed for 6 days. Subsequently, 400 μL of 3-[4,5-dimethyl-2-thiazolyl]-2,5-diphenyl-2*H*-tetrazolium bromide was added to the nanobiocomposites, and TCP was used as the control. Following incubation at 40 °C for 3 h, the active cells take up MTT and forms a purple-colored formazan, which was further dissolved in DMSO (500 μL/well). A microplate spectrophotometer (λ = 570 nm) was used to find out the optical density. Absorbance of cells by nanobiocomposites to that of control cells gives the cell proliferation.[61,62] The cell viability of samples were computed using the equation described below

$$\% \text{ cell viability} = \frac{\text{mean OD}_{\text{Sample}}}{\text{mean OD}_{\text{Blank}}} \times 100$$

The fluorescent microscope was employed for this purpose and the attachment as well as proliferation of 3T3-L1 cells on the prepared NBCs. The procedure of studying cell

morphology and compatibility for the prepared NBCs have been explained in detail in our previous studies.[3]

2.9. Statistical Analysis. Studies on the adherence of 3T3-L1 cells and their proliferation on the prepared NBCs were conducted as triplicates. The data obtained were reported in the form of mean ± standard deviation (SD). Also, the comparison of the data were done using ANOVA and then Duncan multiple test with SPSS 13 software. Those values were $p < 0.05$ were regarded as significant.

3. RESULTS AND DISCUSSION

The CD spectrum of aqueous SC solution exhibited $\pi-\pi^*$ amide and $n-\pi^*$ transitions at 201 and 228 nm, respectively (Figure 1). The intensity of both these bands was compared to
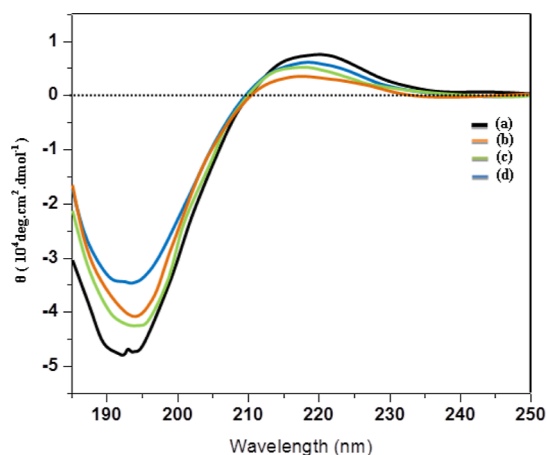

Figure 1. CD spectrum of (a) native collagen, (b) SC, (c) FDSC, and (d) FFCSC, respectively.

determine the triple helical content of collagen molecules and matched well with that of unmodified collagen. From the CD spectra, the ratio between positive and negative peaks (R_{pn}) was obtained for native and modified collagen solution are provided in Table 1. The R_{pn} value for native collagen was

Table 1. R_{pn} Values for Native Collagen C, SC, FDSC, and FFCSC NBCs Respectively

sample	R_{pn} value
collagen	0.106
SC	0.13
FDSC	0.12
FFCSC	0.14

0.106, whereas for SC, it was found to be 0.13. The process of succinylation resulted in the increased R_{pn} value. The incorporation of Fe_3O_4 NPs in FDSC and FFCSC shows no significant alterations in the CD spectra, which confirms the absence of conformational changes in the collagen structure, respectively. Therefore, the R_{pn} value for FDSC was 0.12, similar to that of native collagen. However, in FFCSC, it was found to be 0.14 which can be attributed to the crosslinking effect with SC and also indicates that the maximum stabilization effect on the native conformation of collagen molecule was exerted by FFCSC. The findings are in accordance with the earlier reported works.[63,64]

The particle size of the bare and aminosilane-functionalized Fe_3O_4 NPs (from PSA) was 10−40 nm (Figure 2). The
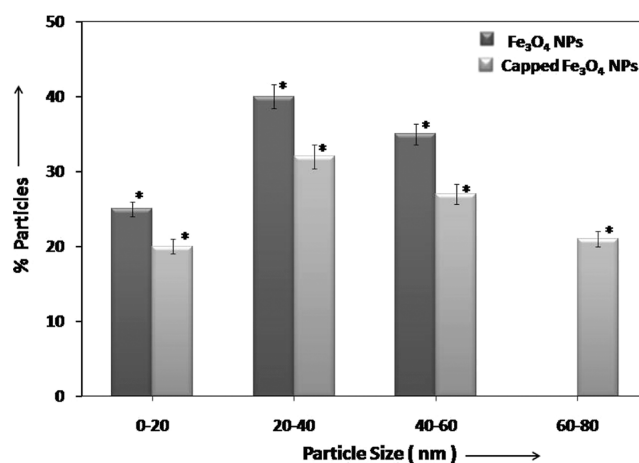

Figure 2. Particle size distribution of bare and functionalized Fe_3O_4 NPs.

information on the structural parameters for the prepared nanoparticles was acquired by XRD. The XRD prototypes found for both bare and aminosilane-functionalized nanoparticles are in agreement with the reference sources.[65−67]

The peaks at $2\theta = 31, 35.5, 43, 53.5, 57$, and 62° matched with JCPDS card no. 85-1436 are due to (200), (311), (400), (422), (511), and (440) Bragg reflections, confirms Fe_3O_4 with cubic spinel arrangement[67] (see Figure 3). Also, the particle size calculated for bare and aminosilane-capped Fe_3O_4 NPs from well-known Scherrer's equation: $d = K\lambda/\beta \cos \theta$.[66]
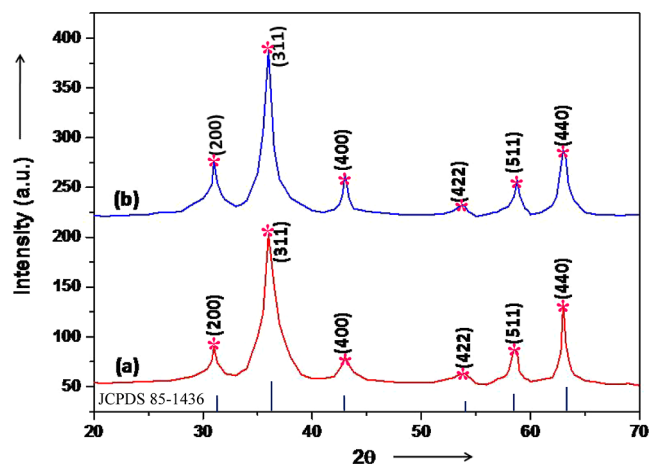

Figure 3. XRD graph of (a) bare and (b) aminosilane-functionalized Fe_3O_4 NPs.

The diameter values obtained were 19 and 31 nm for bare and aminosilane-functionalized Fe_3O_4 NPs, which is following the PSA results. Fe_3O_4 NPs (<10 nm) exhibit quasi-single or single magnetic domain structures that result in super-paramagnetism.[68,69] To compare the magnetic properties between bare Fe_3O_4 NPs and amine-functionalized Fe_3O_4 NPs, their M−H curves at 300 K were measured by a magnetic property measurement system. Figure 4 depicts the M−H curve of bare and functionalized Fe_3O_4 NPs at 300 K. The graph demonstrates superparamagnetism at 300 K as very low values of coercivity and remanence are observed. The saturation magnetization (Ms) value reduces when particle size is lowered courtesy to finite size effect.[67] The Ms of bare Fe_3O_4
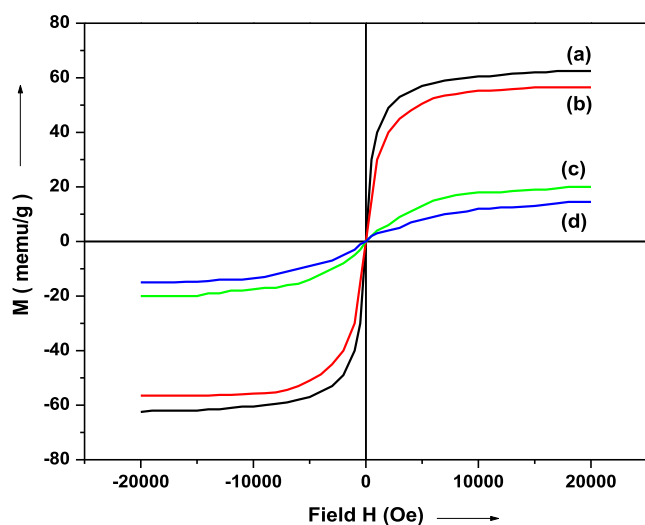
Figure 4. M−H curve of (a) bare Fe_3O_4 and (b) functionalized Fe_3O_4 NPs, (c) FDSC, and (d) FFCSC at 300 K, respectively.
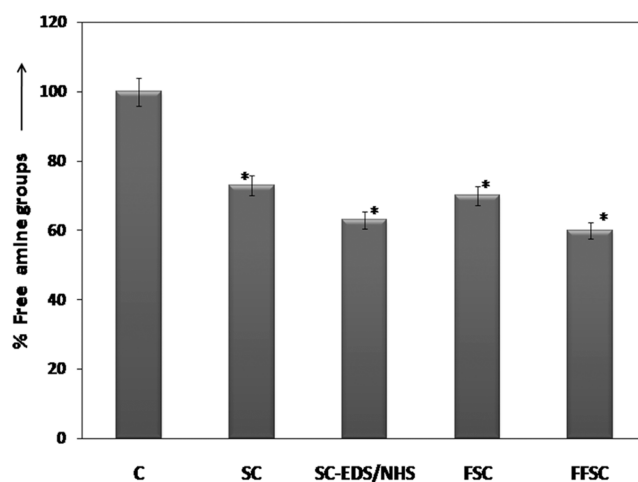

Figure 5. Percentage of amine content of the NBCs produced in this study, concerning non-cross-linked collagen scaffolds. Values are presented as mean $\pm$ SD ($n = 3$).
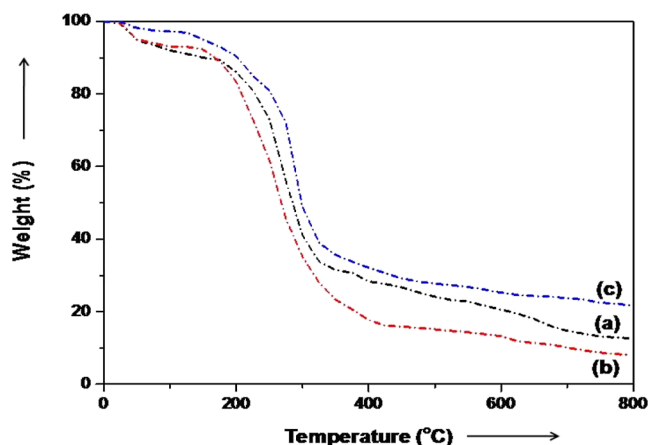

Figure 6. TGA of nanobiocomposites: (a) SC, (b) FDSC, and (c) FFCSC, respectively.

NPs was observed at 61.8 memu/g but it was lowered to 56.5 memu/g for functionalized Fe_3O_4 NPs. This observation could be due to the more pronounced surface disorder and modified cationic distribution noted for smaller-sized particles that restrict the core spins to align with the field and results in lower saturation magnetization. Thus, magnetic measurements on both Fe_3O_4 NPs (before and after functionalization) indicate that the particles are superparamagnetic at 300 K and the net magnetization of the particles is zero even without an external field. The superparamagnetic properties exerted by the Fe_3O_4 NPs play a crucial role in magnetic composites that have biomedical applications. It is well established that these Fe_3O_4 NPs present effective mechanical stimulation under an external magnetic field and facilitate tissue regeneration.[32] The Ms value decreases after incorporating Fe_3O_4 NPs into the SC matrix and was found to be the least in the case of FFCSC. This can be attributed to the entanglement of the collagen fibers that cover the magnetic domains of functionalized Fe_3O_4 NPs and formed chemical bonds with SC, respectively. Also, it can be summarized that lower Ms value for FFCSC can be correlated to the reduced porosity and increased tensile strength of the NBC, respectively. The Fe_3O_4 NPs stability in solution was assessed with zeta potential measurements. It is noteworthy to mention here that the stability of the NPs is of utmost essential for their application in medical fields.[70] Zeta potential of -23.2 mV for bare Fe_3O_4 NPs shows that solution is stable for a long time. Similarly, aminosilane-capped Fe_3O_4 NPs exhibit a zeta potential of $+18.6$ mV. Aminosilane is responsible for providing stabilization and controls the movement of iron ions during the reaction and prevents aggregation.[24]

The high zeta potential value is due to electrostatic repulsion between NPs and this avoids their deposition and results in highly stable NPs. Ninhydrin assay evaluated the free amino groups on the collagen nanobiocomposites, and the result is illustrated in Figure 5. EDC/NHS cross-linking showed lower number of free amines (63%) than the FDSC (70%) and SC (73%). The free amine content further decreased in the case of the FFCSC nanobiocomposites (61%).

3.1. Physico-Chemical Properties of the Nanobio-composites. The thermal stabilities of the samples: SC, FDSC, and FFCSC were determined by TGA. In Figure 6, the

decomposition monitored for SC, FDSC, and FFCSC can be divided into two steps. The first step occurs at temperatures below 100 °C, where the mass loss is attributed to evaporation of low-molecular-weight compounds, that is, mainly due to adsorbed water.[6,71] At comparable temperatures, say 80 °C, samples showed mass loss are 5.6, 5.0, and 2.5%, for SC, FDSC, and FFCSC, respectively. The FFCSC degradation (6.5%) occurred at temperatures above 170 °C, while SC and FDSC showed mass losses as 10.1 and 7.8%, respectively. Most of the degradation takes place between 400 and 500 °C and shows mass loss of 83.5, 72.2, and 64% in SC, FDSC, and FFCSC, respectively. Furthermore, to complement the TGA data obtained for samples, SC, FDSC, and FFCSC, DSC technique was also employed (Figure 7). There were three peaks in both SC and FDSC. For SC, it was found to be 91, 152, and 216 °C having activation energies of 42.1, 56, and 183 J/g, respectively. For FDSC, the calculated activation energies were found to be 306.6, 11.5, and 16.8 J/g for respective peaks at 85, 172, and 251 °C. However, there were four peaks obtained in the case of FFCSC at 94, 134, 189, and 225 °C, whose activation energies were 21.3, 10.7, 8.3, and 59.3 J/g, respectively.

The higher values of transition temperatures suggest that the collagen-based nanobiocomposites are stable. The high
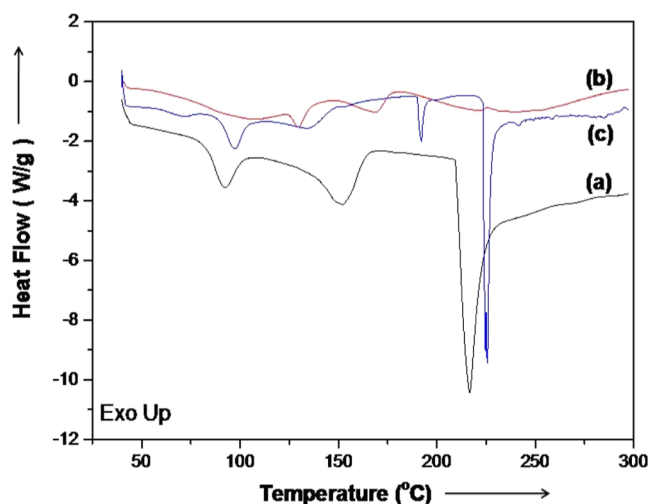
Figure 7. DSC analysis of nanobiocomposites: (a) SC, (b) FDSC, and (c) FFCSC, respectively.

thermal stability affects the collagen-based nanobiocomposites and also accounts for their durability. Also, the melting temperature was also recorded and it was found to be SC (91 °C), FDSC (85 °C), and FFCSC (94 °C), as shown in Figure 7. Overall, the above-mentioned analytical techniques demonstrate FFCSC as more stable than SC and FDSC. Besides, this the final residue (%) that remained above 600 K was more in FFCSC (21.8%) than that in SC (12.6%).

FT-IR spectroscopy, the versatile technique to characterize and study the interaction between Fe_3O_4 NPs and collagen. Figure 8 shows FT-IR spectra of SC alone, FDSC, and FFCSC
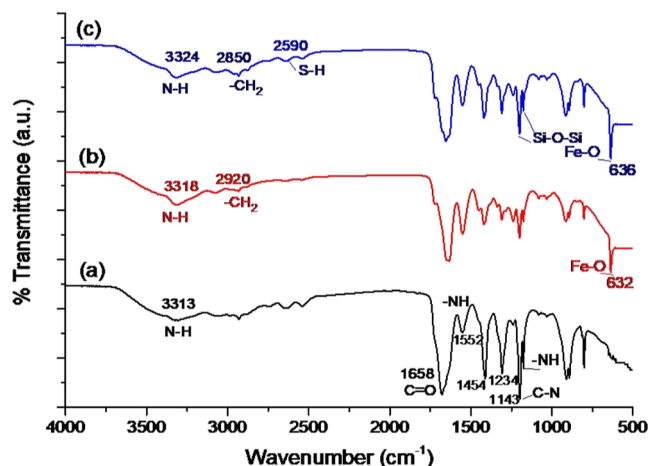

Figure 8. FTIR spectra of nanobiocomposites: (a) SC, (b) FDSC, and (c) FFCSC, respectively.

nanobiocomposites. The Fe_3O_4 NPs peak usually noticed due to the Fe−O bond formation at 580 cm^{-1} had shifted to 632 and 636 cm^{-1} in FDSC and FFSC, respectively.[26] The blueshift can be ascribed to the Fe_3O_4 NPs in collagen that was monodispersive with the precursors.[60] The broadening and higher shift in the band due to Fe−O−Si bonds was observed in FFCSC.[72] S−H stretch vibration band due to mercaptosilane in amino-functionalized Fe_3O_4 NPs was noted at 2590 cm^{-1}. Also, additional bands are noticed for silane-modified Fe_3O_4 NPs compared to the uncoated NPs. The bands between 1000 and 1150 cm^{-1} are due to Si−O−Si

vibrations for siloxanes. Here, in this case, it is due to the condensation of siloxane (Si−O) molecules onto the surface of the magnetic, Fe_3O_4 NPs.[73] Moreover, in FFSC, low-intensity bands, 1300−1600 cm^{-1} associated to both free and bound aminopropyl segment, which can be overlapped by the OH band are observed. The 1491 cm^{-1} peak is due to the symmetric deformation mode of the −NH$_3^+$ group.[74] The amino-silane also shows two N−H bendings at 1633 and 1571 cm^{-1}, characteristic of the presence of NH$_3^+$ groups.[60] The peaks at 1515 and 1421 cm^{-1}, are due to interactions of oleic acid with iron oxide. Also, an additional vibration band at 1348 cm^{-1} validates the oleylamine bound on the surface of Fe_3O_4 NPs.[48] Moreover, FTIR spectra of FDSC and particularly FFCSC displayed the distinctive vibration bands at 2850 and 2920 cm^{-1} are due to amide bond formation. This confirms the linkage of the SC with that of the antisymmetric −CH$_2$ moieties of ole amine present in synthesized magnetic NPs to form covalent bond formation. The FT-IR spectra also showed all the main amide peaks; noticed at 1654 cm^{-1} (amide I C═O stretching), 1554 cm^{-1} (amide II N−H stretching), and between 1140 and 1315 cm^{-1} due to amide III (C−N and N−H stretching).

These peaks confirm the retainment of the collagen structure. Moreover, the T_{1454}/T_{1234} ratio has a value close to unity in all the nanobiocomposites, indicating the conservation of the triple helical conformation of collagen formed in the covalent networks.[75] The band at 1450 cm^{-1} is due to C−H bending and the amide band (symmetric N−H stretching) observed at 3311 cm^{-1}, which suggests that the water is present in traces.[27,76] X-ray photoelectron spectroscopy (XPS) provides vital information on the binding modes/mechanism of bimetallic nanoparticles with that of biomaterial.[77] A separate study will be carried out using computational (DFT) and XPS techniques to ascertain the attachment of Fe_3O_4 NPs with that of collagen in detail. In FT-IR spectra (Figure 8), the peak appeared at 3313 cm^{-1} for SC and the interactions between SC and aminosilane-functionalized Fe_3O_4 NPs are associated with the occurrence of peak at 3324 cm^{-1} (FFCSC). This peak is shifted to 3318 cm^{-1} in the case of FDSC. The broad peak is due to the interactions between the hydroxyl groups of SC and partial positive charge on the surface of Fe_3O_4 NPs.[53,54] The amide band (−NH stretching) observed at 3324 cm^{-1} is almost symmetric, which suggests that the amount of water present is low.[52,78] However, intermolecular H-bonding may not be ruled out. The micelle formation on collagen in acetic acid/acetate buffer and its interactions with various surfactant micelles and urea had been discussed thoroughly by Mandal et al.[79−81] in the light of aggregation, shape, size, hydrations, conformations, and thermodynamic studies. Both one hydrogen bonded and two hydrogen bonded models were discussed. The aggregation, H bonding, and thermodynamic studies in tetra-peptide and tri-peptide micelle in aqueous and non-aqueous solvent were reported in the past[82,83] where the temperature dependence proton chemical shift, i.e., (dδ/dT), will dictate whether strong covalent bond (intramolecular) or weak H-bond (intermolecular) takes place. Therefore, in our present FTIR spectra, it is difficult to predict clearly. Further studies using temperature dependence ^{1}H NMR in this direction would be interesting.

3.2. Mechanical Properties. The mechanical characteristics of the developed collagen-based nanobiocomposites were also studied with respect to SC to ensure whether the biomaterial will be intact during clinical applications. The

percentage elongation at break of 48.1% was noticed for FFCSC nanobiocomposites; while the value was lower in the case of FDSC nanobiocomposites (31%) and the minimum percentage, i.e., 23% was observed with the SC nano-biocomposite. The tensile strengths of SC, FDSC, and FFCSC nanobiocomposites were found to be 1.1 ± 0.31, 1.45 ± 0.61, and 5.3 ± 0.71 MPa, respectively (see Figure 9).
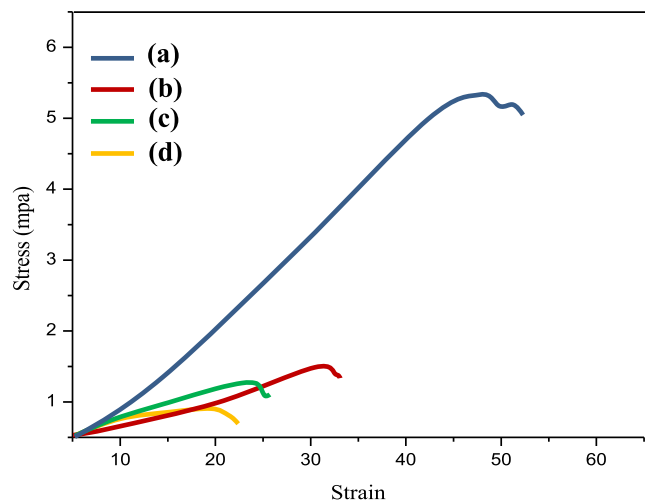

Figure 9. Stress strain curve for collagen-based NBCs: (a) FFCSC, (b) FDSC, (c) SC, and (d) collagen alone, respectively.

Hence, the cross-linked product lead increased the tensile strength by fivefold in comparison with SC. The results thus imply that surface-modified Fe_3O_4 NPs crosslinked with collagen increase the elasticity, useful to prepare artificial heart valves. The nanobiocomposite porosity was calculated by following the protocol employed by Shimizu et al.[36] The porosities of the SC, FDSC, and FFCSC nanobiocomposites were 95.42 ± 0.37, 93.17 ± 0.45, and 91.94 ± 0.77%, respectively. In the current investigation, collagen derived from the fish scales was succinylated and used. It is to be noted that no drastic change in mechanical stability results for SC doped with iron oxide (FDSC) when compared to SC. However, in the case of SC functionalized and cross-linked with iron oxide (FFCSC), the mechanical strength in addition to the thermal stability was significantly enhanced. From our understanding, not many reports exist on collagen cross-linking with succinic acid. It is well known that amine groups present in the proteins such as collagen (lysyl ε-NH_2) are powerful nucleophiles, which react with a carbonyl group ($-C{=}O$) to form covalent bonds via the nucleophilic addition−elimination reaction.[84] However, in the present study, ionic interaction takes place which can be described as follows: succinic acid protonates $-NH_2$ groups of collagen and the resulting $-NH_3^+$ sites interact with $-COO^-$ of succinic acid to form stronger biocomposites. The presence of Fe cations enhances the transformation process. SEM images as illustrated in Figure 10(b,c) show that there was no significant agglomeration, courtesy to the substitution of ligand oleic acid with APTMS that occur on the nanoparticles surface. The EDAX spectrum has a strong signal of Fe. Also, observed signals of C, O, Cl, and Si (Figure 10d) are due to the coating process involved for Fe_3O_4 NPs.

TEM images of the NBCs, FDSC, and FFCSC reveal that the Fe_3O_4 NPs were well dispersed on the collagen surface (see

Figure 11). Moreover, the size of Fe_3O_4 was found to less than 50 nm which is in accordance with PSA and XRD results. Slight aggregation of Fe_3O_4 NPs was noticed in FFCSC due to crosslinking of the collagen fibers. A similar kind of effect was noticed for chitosan rods when reinforced in multiwalled carbon nanotubes.[85]

3.3. Biological Properties. To evaluate the prepared biomaterial for its use as implants, it is vital to assess the biodegradability. So, the collagen nanobiocomposites cross-linked with surface-modified Fe_3O_4 NPs were treated with collagenase enzyme and their rate of degradation was monitored. The collagenase enzyme is responsible for the release of hydroxyproline from the nanobiocomposites. The experiment was monitored for 108 h and the result is shown in Figure 12. The hydroxyproline released from the nano-biocomposites after 24 h of treatment with collagenase did not show any drastic change. However, a significant difference was noticed from 12 to 24 h where the release of hydroxyproline of SC is higher compared to FDSC and FFCSC nanobiocomposites. Therefore, it can be confirmed that all the nanobiocomposites developed are biodegradable when treated with collagenase. The MIC for nanobiocompo-sites, FDSC, and FFCSC were determined for both types of bacterial strains concerning SC as control is shown in Figure 13.

The MIC value for SC was 350 ± 11 μg/mL for *E. coli*, whereas the increased value of 425 ± 17 μg/mL was observed for Gram-positive strain, *S. aureus*. The FFCSC nano-biocomposites displayed lower MIC in comparison to Fe_3O_4 NPs impregnated in SC nanobiocomposites (FDSC). For Gram-negative bacteria, *E. coli*, FFCSC demonstrated a value of 232 ± 7 μg/mL, lower than FDSC nanobiocomposites, which exhibited 275 ± 12 μg/mL, respectively. A similar trend for Gram-positive bacteria, *S. aureus*, was observed, where 317 ± 11 μg/mL for FFCSC in comparison to 345 ± 16 μg/mL for NBCs: SC that contains Fe_3O_4 NPs was noted. The superior antibacterial outcome in *E. coli* is due to its lack of cell membrane where the Fe_3O_4 NPs easily infiltrate and act with cellular contents to inhibit bacterial growth. It is well documented that the surface immobilization of nanoparticles leads to more contact and so kills the bacteria effectively compared to colloidal ones.[86] Thus, FFCSC exhibits improved efficacy than FDSC that can be used in tissue engineering applications.

3.4. In Vitro Studies: Viability and Morphology of 3T3-L1 Cells. The surface chemistry and topography are major factors that govern and regulate cell behavior, which decides if the nanobiocomposites can behave as scaffolds. The proliferation of 3T3-L1 on FDSC and FFCSC cultured for 6 days was evaluated from MTT assay, and results are provided in Figure 14.

For the proliferation of the fibroblast, both FDSC and FFCSC had superior cell viability than SC. Among the nanobiocomposites, FDSC showed a marginal increase in the proliferation rate compared to FFCSC. SEM images of both FDSC and FFCSC nanobiocomposites seeded with 3T3-L1 cells on days 2 and 6 were compared with SC nano-biocomposites and examined to investigate their morphology (see Figure 15). It is obvious from the SEM depicted in Figure 15c−f which show both the nanobiocomposites FDSC and FFCSC, facilitated the proliferation of the 3T3-L1 cells required for tissue formation and thereby the nanobiocompo-site provide a matrix and acts as scaffolds. Similarly,
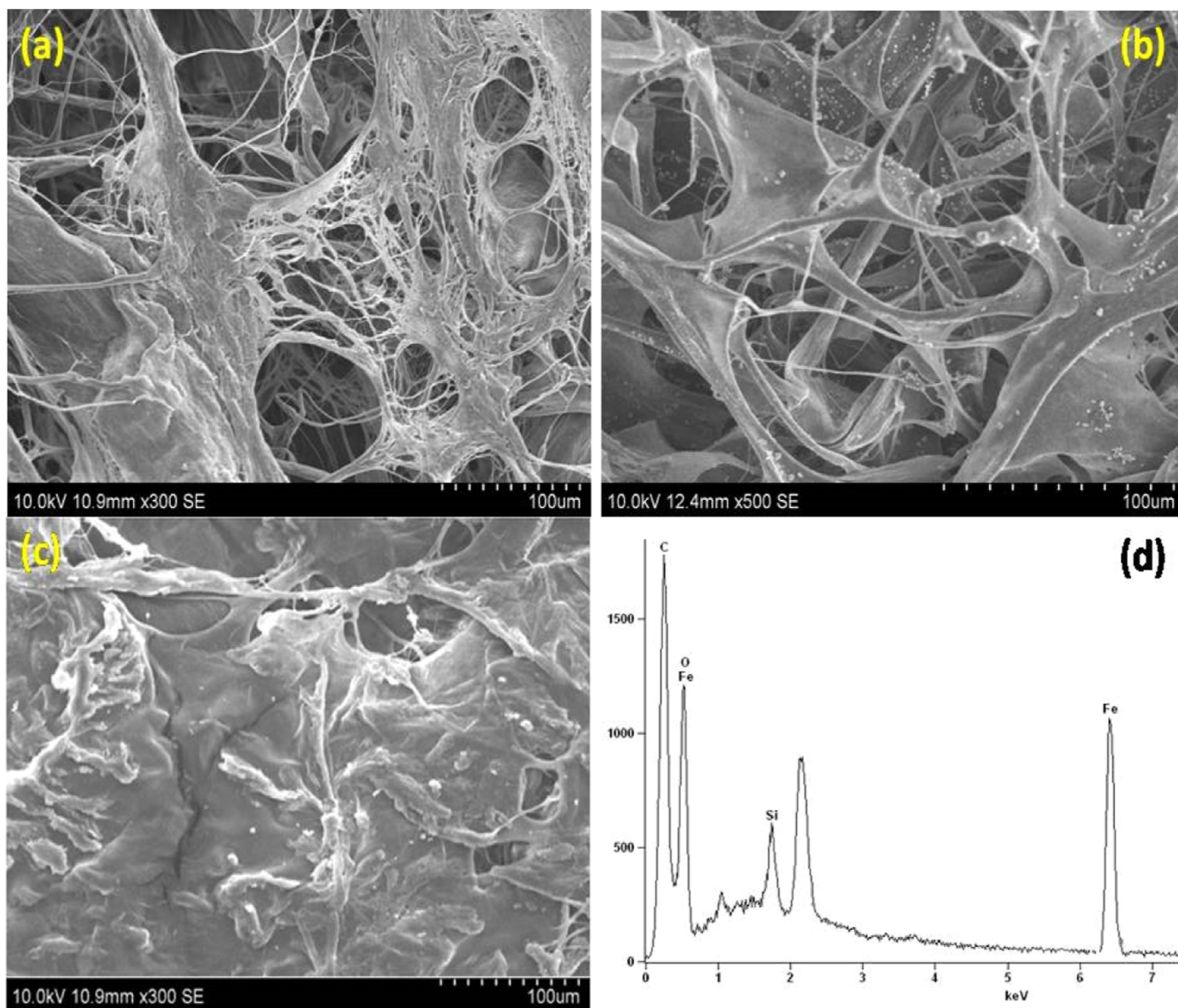
Figure 10. SEM images of (a) SC, (b) FDSC, and (c) FFCSC NBCs, respectively. (d) Elemental composition of FFCSC NBCs using energy dispersive X-ray spectroscopy.
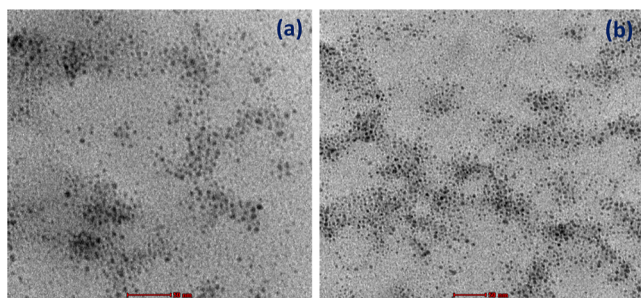

Figure 11. TEM images of (a) FDSC and (b) FFCSC NBCs, respectively.

fluorescence micrographs of 3T3-L1 cells were taken after 48 h of culture on the nanobiocomposites: SC, FDSC, and FFCSC (see Figure 16). The presence of Fe_3O_4 NPs in FDSC and FFCSC nanobiocomposites most likely modulate the orientation of collagen fibers to enhance cell differentiation and proliferation.[87]
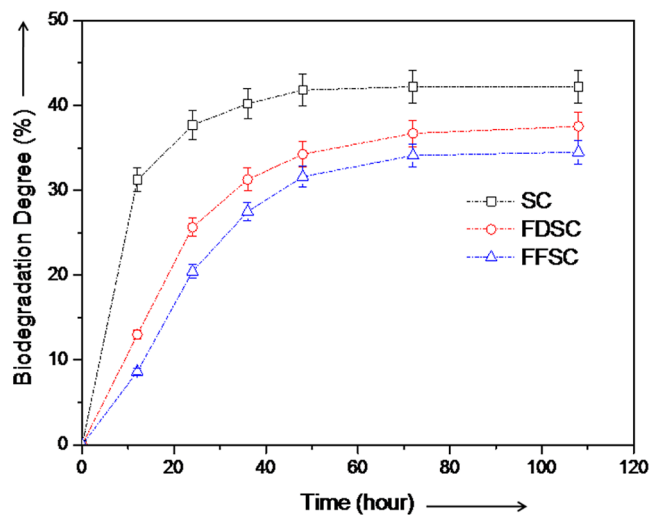

Figure 12. Biodegradability assessment based on the release of hydroxyproline from SC, FDSC, and FFCSC nanobiocomposites.
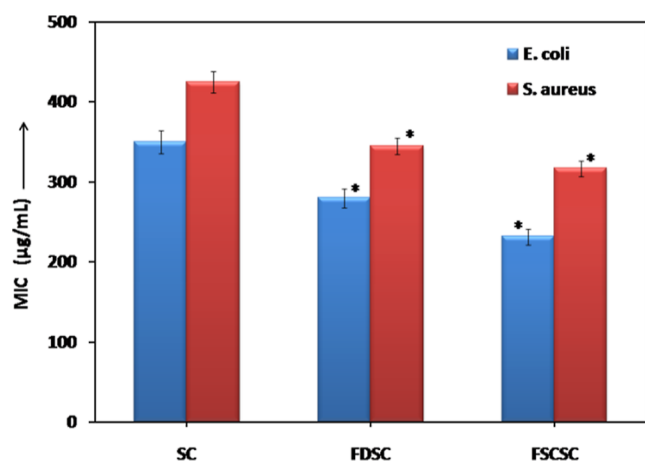
Figure 13. MIC for FDSC and FFCSC nanobiocomposites tested against both Gram-positive and -negative bacterial strains compared to SC used as the control. The asterisks indicate statistically significant differences compared to the control ($p < 0.05$).
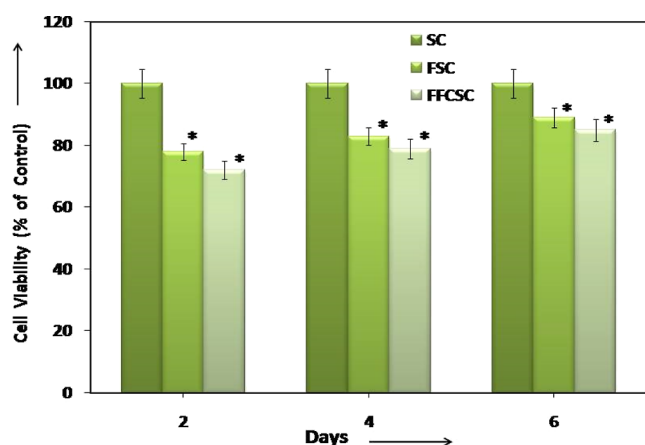
Figure 14. MTT assay illustrates the cell viability of fibroblast (3T3-L1) cells on SC, FSC, and FFCSC nanobiocomposites, respectively. The asterisks indicate statistically significant differences compared to the control ($p < 0.05$).

Figure 15. Evaluation of biocompatibility after 2 and 6 days for SC (a,b), FSC (c,d), and FFCSC (e,f) nanobiocomposites, respectively, with 3T3-L1 cells, captured by SEM.

Figure 16. Fluorescence micrographs (20×) of 3T3-L1 cells captured after 48 h of culture on (a) SC, (b) FDSC, and (c) FFCSC nanobiocomposites, respectively. All scale bars are 200 μm.

4. CONCLUSIONS

The present investigation reports the fabrication of thermally stable biopolymer material from collagen obtained from scales of *Lates Calcarifer*, a marine origin, and succinic acid which enhanced the thermal properties on cross-linking with Fe_3O_4 NPs. The amino groups in APTMS functionalize magnetic nanoparticles and enables them toward cross-linking to collagen by succinylation. Detailed characterization to understand the physicochemical properties of the fabricated nanobiocomposites FFCSC were carried and assessed with FDSC. The VSM result confirms the magnetic property of both Fe_3O_4 and functionalized Fe_3O_4 NPs. The DSC/TGA analyses indicate more stability of FFCSC than FDSC attributed to the cross-linking effects. Additionally, improved mechanical and biodegradation properties were noticed in FFCSC as compared to the FDSC nanobiocomposite. Enzymatic degradation of FFCSC, FDSC, and SC nanobiocomposites was studied, and the results showed that all the nanobiocomposites degraded when treated with the collagenase enzyme. Morphology and viability data of 3T3-L1 cells suggest both FDSC and FFCSC nanobiocomposites as 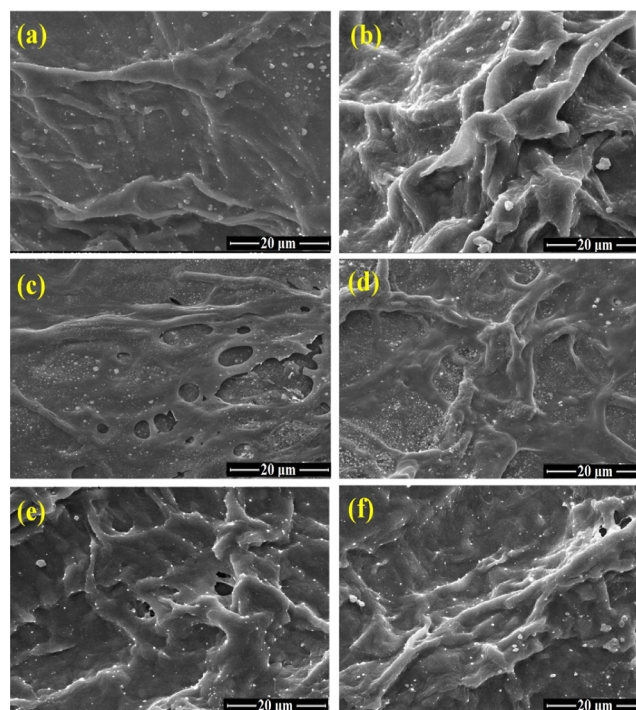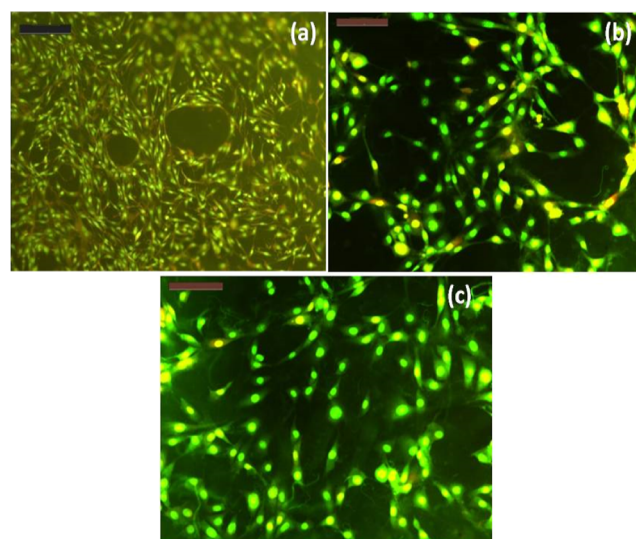compatible that is apt for biomedical purposes. However, the cell viability of FDSC nanobiocomposites with fibroblast cells showed a marginal increase in the proliferation rate than the FFCSC nanobiocomposite. Hence, it is noteworthy to state that both FDSC and specially FFCSC could find potential applications as a MRI contrast agent and possibly in targeted therapeutics, as the nanoparticles are water soluble and also biocompatible. Moreover, better attachment with biomolecules like collagen is facilitated by the amino groups present on Fe_3O_4 NPs surface (FFCSC) and can be further used for labeling cells in cancer therapy. Therefore, in this study, the collagen-based nanobiocomposites incorporated with Fe_3O_4

NPs (FFCSC and FDSC) present a straight forward, clean, and effective method for the renewal and recycle of the bio-waste to value-based materials that have potential biomedical applications.

■ AUTHOR INFORMATION

Corresponding Authors

Abhishek Mandal — *Department of Physical Chemistry, School of Chemical Sciences, University of Madras, Chennai 600 025, India; Department of Biotechnology, School of Life Sciences, Pondicherry University, Puducherry 605 014, India;* orcid.org/0000-0003-0392-3620; Phone: +91-6382838326; Email: abhishek.m@pondiuni.ac.in

Eagambaram Murugan — *Department of Physical Chemistry, School of Chemical Sciences, University of Madras, Chennai 600 025, India;* orcid.org/0000-0001-9751-9690; Phone: +91-9444275889; Email: dr.e.murugan@gmail.com

Author

Ezhumalai Dhineshkumar — *Dr. Krishnamoorthi Foundation for Advanced Scientific Research, Vellore 632 001 Tamil Nadu, India*

Complete contact information is available at:
https://pubs.acs.org/10.1021/acsomega.3c01106

Notes

The authors declare no competing financial interest.

■ REFERENCES

(1) Mandal, A.; Meda, V.; Zhang, W. J.; Farhan, K. M.; Gnanamani, A. Synthesis, characterization and comparison of antimicrobial activity of PEG/TritonX-100 capped silver nanoparticles on collagen scaffold. *Colloids Surf., B* **2012**, *90*, 191−196.

(2) Yang, J.; Ding, C.; Tang, L.; Deng, F.; Yang, Q.; Wu, H.; Chen, L.; Ni, Y.; Huang, L.; Zhang, M. Novel Modification of Collagen: Realizing Desired Water Solubility and Thermostability in a Conflict-Free Way. *ACS Omega* **2020**, *5*, 5772−5780.

(3) Mandal, A.; Sekar, S.; Seeni Meera, K. M.; Mukherjee, A.; Sastry, T. P.; Mandal, A. B. Fabrication of collagen scaffolds impregnated with sago starch capped silver nanoparticles suitable for biomedical applications and their physicochemical studies. *Phys. Chem. Chem. Phys.* **2014**, *16*, 20175−20183.

(4) Furtado, M.; Chen, L.; Chen, Z.; Chen, A.; Cui, W. Development of fish collagen in tissue regeneration and drug delivery. *Engineered Regeneration* **2022**, *3*, 217−231.

(5) Sripriya, R.; Kumar, R.; Balaji, S.; Senthil Kumar, M.; Sehgal, P. K. Characterizations of polyanionic collagen prepared by linking additional carboxylic groups. *React. Funct. Polym.* **2011**, *71*, 62−69.

(6) Mandal, A.; Katheem Farhan, M.; Sastry, T. P. Effect of reinforced Al_2O_3 nanoparticles on collagen nanobiocomposite from chrome-containing leather waste for biomedical applications. *Clean Technol. Environ. Policy* **2016**, *18*, 765−773.

(7) Rajabimashhadi, Z.; Gallo, N.; Salvatore, L.; Lionetto, F. Collagen Derived from Fish Industry Waste: Progresses and Challenges. *Polymers* **2023**, *15*, 544.

(8) Iwamoto, Y.; Haraguchi, R.; Nakao, R.; Aoki, S.; Oishi, Y.; Narita, T. One-pot preparation of collagen tubes using diffusing gelation. *ACS Omega* **2022**, *7*, 22872−22878.

(9) Mekonnen, B. T.; Ragothaman, M.; Palanisamy, T. Bifunctional hybrid composites from collagen biowastes for heterogeneous applications. *ACS Omega* **2017**, *2*, 5260−5270.

(10) Wang, Y.; Wang, Z.; Dong, Y. Collagen-Based Biomaterials for Tissue Engineering. *ACS Biomater. Sci. Eng.* **2023**, *9*, 1132−1150.

(11) Alfio, V. G.; Manzo, C.; Micillo, R. From Fish Waste to Value: An overview of the sustainable recovery of Omega-3 for food supplements. *Molecules* **2021**, *26*, 1002.

(12) Perveen, F.; Farooq, M.; Naeem, A.; Humayun, M.; Saeed, T.; Khan, I. W.; Abid, G. Catalytic conversion of agricultural waste biomass into valued chemical using bifunctional heterogeneous catalyst: A sustainable approach. *Catal. Commun.* **2022**, *171*, 106516.

(13) Sankar, S.; Sekar, S.; Mohan, R.; Rani, S.; Sundaraseelan, J.; Sastry, T. P. Preparation and partial characterization of collagen sheet from fish (Lates calcarifer) scales. *Int. J. Biol. Macromol.* **2008**, *42*, 6−9.

(14) Milan, E. P.; Bertolo, M. R. V.; Martins, V. C. A.; Sobrero, C. E.; Plepis, A. M. G.; Fuhrmann-Lieker, T.; Horn, M. M. Effects of Mangosteen Peel Phenolic Compounds on Tilapia Skin Collagen-Based Mineralized Scaffold Properties. *ACS Omega* **2022**, *7*, 34022−34033.

(15) Garcia-Sanda, E.; Omil, F.; Lema, J. M. Clean production in fish canning industries: recovery and reuse of selected wastes. *Clean Technol. Environ. Policy* **2003**, *5*, 289−294.

(16) Tay, C.; Muda, A.; Abdul-Talib, S.; Ab-Jalil, M.; Othman, N. The half saturation removal approach and mechanism of Lead (II) removal using eco-friendly industrial fish bone meal waste biosorbent. *Clean Technol. Environ. Policy* **2016**, *18*, 541−551.

(17) Liu, C.; Sun, J. Impact of Marine-Based Biomaterials on the Immuno regulatory Properties of Bone Marrow-Derived Mesenchymal Stem Cells: Potential Use of Fish Collagen in Bone Tissue Engineering. *ACS Omega* **2020**, *5*, 28360−28368.

(18) Perez-Galvez, R.; García-Moreno, P. J.; Huong, N. T.; Guadix, E. M.; Guadix, A. J.; Bergé, J. P. Multiobjective optimization of a pilot plant to process fish discards and by-products on board. *Clean Technol. Environ. Policy* **2016**, *18*, 935−948.

(19) Chinh, N. T.; Manh, V. Q.; Trung, V. Q.; Lam, T. D.; Huynh, M. D.; Tung, N. Q.; Trinh, N. D.; Hoang, T. Characterization of aollagen derived from tropical freshwater carp fish scale wastes and its amino acid sequence. *Nat. Prod. Commun.* **2019**, *14*, 1934578X19866288.

(20) Pati, F.; Datta, P.; Adhikari, B.; Dhara, S.; Ghosh, K.; Mohapatra, P. K. D. Collagen scaffolds derived from fresh water fish origin and their biocompatibility. *J. Biomed. Mater. Res., Part A* **2012**, *100*, 1068−1079.

(21) Subhan, F.; Ikram, M.; Shehzad, A.; Ghafoor, A. Marine Collagen: An emerging player in biomedical applications. *J. Food Sci. Technol.* **2015**, *52*, 4703−4707.

(22) Yang, J.; Ding, C.; Tang, L.; Deng, F.; Yang, Q.; Wu, H.; Chen, L.; Ni, Y.; Huang, L.; Zhang, M. Novel Modification of collagen: Realizing desired water solubility and thermostability in a conflict-free way. *ACS Omega* **2020**, *5*, 5772−5780.

(23) Castaneda, L.; Valle, J.; Yang, N.; Pluskat, S.; Slowinska, K. Collagen Crosslinking with Au Nanoparticles. *Biomacromol* **2008**, *9*, 3383−3388.

(24) Mandal, A.; Sekar, S.; Chandrasekaran, N.; Mukherjee, A.; Sastry, T. P. Synthesis, characterization and evaluation of collagen scaffolds crosslinked with aminosilane functionalized silver nanoparticles: in vitro and in vivo studies. *J. Mater. Chem. B* **2015**, *3*, 3032−3043.

(25) Jafari, H.; Lista, A.; Siekapen, M. M.; Ghaffari-Bohlouli, P.; Nie, L.; Alimoradi, H.; Shavandi, A. Fish Collagen: Extraction, Character-

ization, and Applications for Biomaterials Engineering. *Polymers* **2020**, *12*, 2230.

(26) Hollecker, M.; Creighton, T. E. Counting integral numbers of amino groups per polypeptide chain. *FEBS Lett.* **1980**, *119*, 187−189.

(27) Mandal, A.; Sekar, S.; Chandrasekaran, N.; Mukherjee, A.; Sastry, T. P. Vibrational spectroscopic investigation on interaction of sago starch capped silver nanoparticles with collagen: a comparative physicochemical study using FT-IR and FT-Raman techniques. *RSC Adv.* **2015**, *5*, 15763−15771.

(28) Rico-Llanos, G. A.; Borrego-González, S.; Moncayo-Donoso, M.; Becerra, J.; Visser, R. Collagen type I biomaterials as scaffolds for bone tissue engineering. *Polymers* **2021**, *13*, 599.

(29) Yang, H.; Chen, Y.; Chen, Z.; Geng, Y.; Xie, X.; Shen, X.; Li, T.; Li, S.; Wu, C.; Liu, Y. Chemo-photodynamic combined gene therapy and dual-modal cancer imaging achieved by pH-responsive alginate/chitosan multilayer-modified magnetic mesoporous silica nanocomposites. *Biomater. Sci.* **2017**, *5*, 1001−1013.

(30) Wang, H.; Zhou, S. Magnetic and fluorescent carbon-based nanohybrids for multi-modal imaging and magnetic field/NIR light responsive drug carriers. *Biomater. Sci.* **2016**, *4*, 1062−1073.

(31) Zhang, H.; Patel, N.; Ding, S.; Xiong, J.; Wu, P. Theranostics for hepatocellular carcinoma with Fe_3O_4@ZnO nanocomposites. *Biomater. Sci.* **2016**, *4*, 288−298.

(32) Yan, Y.; Zhang, Y.; Zuo, Y.; Zou, Q.; Li, J.; Li, Y. Development of Fe_3O_4−HA/PU superparamagnetic composite porous scaffolds for bone repair application. *Mater. Lett.* **2018**, *212*, 303−306.

(33) Yew, Y. P.; Shameli, K.; Miyake, M.; Ahmad Khairudin, N. B. B.; Mohamad, S. E. B.; Naiki, T.; Lee, K. X. Green biosynthesis of superparamagnetic magnetite Fe_3O_4 nanoparticles and biomedical applications in targeted anticancer drug delivery system: A review. *Arabian J. Chem.* **2020**, *13*, 2287−2308.

(34) Zhuang, J.; Lin, S.; Dong, L.; Cheng, K.; Weng, W. Magnetically actuated mechanical stimuli on Fe_3O_4/mineralized collagen coatings to enhance osteogenic differentiation of the MC3T3-E1 cells. *Acta Biomater.* **2018**, *71*, 49−60.

(35) Shi, Y.; Li, Y.; Coradin, T. Magnetically-oriented type I collagen-SiO_2@Fe_3O_4 rods composite hydrogels tuning skin cell growth. *Colloids Surf., B* **2020**, *185*, 110597.

(36) Shimizu, K.; Ito, A.; Honda, H. Enhanced cell-seeding into 3D porous scaffolds by use of magnetite nanoparticles. *J. Biomed. Mater. Res., Part B* **2006**, *77*, 265−272.

(37) Liao, N.; Wu, M.; Pan, F.; Lin, J.; Li, Z.; Zhang, D.; Wang, Y.; Zheng, Y.; Peng, J.; Liu, X.; Liu, J. Poly (Dopamine) coated superparamagnetic iron oxide nanocluster for noninvasive labeling, tracking, and targeted delivery of adipose Tissue-derived stem cells. *Sci. Rep.* **2016**, *6*, 18746.

(38) Alvarez-Berrios, M. P.; Castillo, A.; Merida, F.; Mendez, J.; Rinaldi, C.; Torres-Lugo, M. Enhanced proteotoxic stress: one of the contributors for hyperthermic potentiation of the proteasome inhibitor bortezomib using magnetic nanoparticles. *Biomater. Sci.* **2015**, *3*, 391−400.

(39) Mandal, A.; Sekar, S.; Kanagavel, M.; Chandrasekaran, N.; Mukherjee, A.; Sastry, T. Collagen based magnetic nanobiocomposite as MRI contrast agent and for targeted delivery in cancer therapy. *Biochim. Biophys. Acta* **2013**, *1830*, 4628−4633.

(40) Ding, Z.; Liu, P.; Hu, D.; Sheng, Z.; Yi, H.; Gao, G.; Wu, Y.; Zhang, P.; Ling, S.; Cai, L. Redox-responsive dextran based theranostic nanoparticles for near-infrared/magnetic resonance imaging and magnetically targeted photodynamic therapy. *Biomater. Sci.* **2017**, *5*, 762−771.

(41) Liu, S.; Long, L.; Yuan, Z.; Yin, L.; Liu, R. Effect and intracellular uptake of pure magnetic Fe_3O_4 nanoparticles in the cells and organs of lung and liver. *Chin. Med. J.* **2009**, *122*, 1821.

(42) Nelson, N.; Port, J.; Pandey, M. Use of Superparamagnetic Iron Oxide Nanoparticles (SPIONs) via Multiple Imaging Modalities and Modifications to Reduce Cytotoxicity: An Educational Review. *J. Nanotheranostics* **2020**, *1*, 105−135.

(43) Barrow, M.; Taylor, A.; Nieves, D. J.; Bogart, L. K.; Mandal, P.; Collins, C. M.; Moore, L. R.; Chalmers, J. J.; Levy, R.; Williams, S. R.; Murray, P.; Rosseinsky, M. J.; Adams, D. J. Tailoring the surface charge of dextran-based polymer coated SPIONs for modulated stem cell uptake and MRI contrast. *Biomater. Sci.* **2015**, *3*, 608−616.

(44) Gupta, A. K.; Curtis, A. S. Surface modified superparamagnetic nanoparticles for drug delivery: interaction studies with human fibroblasts in culture. *J. Mater. Sci.: Mater. Med.* **2004**, *15*, 493−496.

(45) Fan, M.; Yan, J.; Tan, H.; Miao, Y.; Hu, X. Magnetic biopolymer nanogels via biological assembly for vectoring delivery of biopharmaceuticals. *J. Mater. Chem. B* **2014**, *2*, 8399−8405.

(46) Piñeiro, Y.; González Gómez, M.; de Castro Alves, L.; Arnosa Prieto, A.; García Acevedo, P.; Seco Gudiña, R.; Puig, J.; Teijeiro, C.; Yáñez Vilar, S.; Rivas, J. Hybrid nanostructured magnetite nanoparticles: From bio-detection and theragnostics to regenerative medicine. *Magnetochemistry* **2020**, *6*, 4.

(47) Heinemann, S.; Coradin, T.; Desimone, M. F. Bio-inspired silica−collagen materials: applications and perspectives in the medical field. *Biomater. Sci.* **2013**, *1*, 688.

(48) Achilli, C.; Grandi, S.; Guidetti, G. F.; Ciana, A.; Tomasi, C.; Capsoni, D.; Minetti, G. Minetti Fe_3O_4@SiO_2 core-shell nanoparticles for biomedical purposes: adverse effects on blood cells. *Biomater. Sci.* **2016**, *4*, 1417−1421.

(49) Kumar, S.; Verma, S.; Jain, S. L. Formylation of aromatic iodides using CO_2 as C1 source catalyzed by palladium nanoparticles grafted onto amino-functionalized nano starch. *Tetrahedron Lett.* **2015a**, *56*, 2430−2433.

(50) Lin, S.; Li, J.; Dong, L.; Cheng, K.; Lin, J.; Weng, W. Periodic-Mechanical-Stimulus enhanced osteogenic differentiation of mesenchymal stem cells on Fe_3O_4/mineralized collagen coatings. *ACS Biomater. Sci. Eng.* **2019**, *5*, 6446−6453.

(51) Nguyen, M. D.; Tran, H. V.; Xu, S.; Lee, T. R. Fe_3O_4 Nanoparticles: Structures, Synthesis, Magnetic Properties, Surface Functionalization, and Emerging Applications. *Appl. Sci.* **2021**, *11*, 11301.

(52) Dallas, P.; Bourlinos, A. B.; Niarchos, D.; Petridis, D. Synthesis of tunable sized capped magnetic iron oxide nanoparticles highly soluble in organic solvents. *J. Mater. Sci.* **2007**, *42*, 4996−5002.

(53) Ying, J. Y.; Jana, N. R.; Zheng, Y. Water-soluble, surface functionalized nanoparticle for bioconjugation via universal silane coupling. U.S. Patent 8,097,742 B2, 2012, 5.

(54) Ward, J.; Kelly, J.; Wang, W.; Zeugolis, D. I.; Pandit, A. Amine Functionalization of Collagen Matrices with Multifunctional Polyethylene Glycol Systems. *Biomacromol* **2010**, *11*, 3093−3101.

(55) Chan, J. C.; Burugapalli, K.; Naik, H.; Kelly, J. L.; Pandit, A. Amine functionalization of cholecyst-derived extracellular matrix with generation 1 PAMAM dendrimer. *Biomacromol* **2008**, *9*, 528−536.

(56) Tiong, W. H. C.; Damodaran, G.; Naik, H.; Kelly, J. L.; Pandit, A. Enhancing amine terminals in an amine-deprived collagen matrix. *Langmuir* **2008**, *24*, 11752−11761.

(57) Kesava Reddy, G.; Enwemeka, C. S. A simplified method for the analysis of hydroxyproline in biological tissues. *Clin. Biochem.* **1996**, *29*, 225−229.

(58) Woessner, J. F. The determination of hydroxyproline in tissue and protein samples containing small proportions of this imino acid. *Arch. Biochem. Biophys.* **1961**, *93*, 440−447.

(59) CLSI/NCCLS. *Methods for dilution antimicrobial susceptibility tests for bacteria that grow aerobically; Approved Standard*, 7th ed.; Clinical and Laboratory Standards Institute, 2006.

(60) Mandal, A.; Sekar, S.; Chandrasekaran, N.; Mukherjee, A.; Sastry, T. P. Poly(ethylene) glycol-capped silver and magnetic nanoparticles: Synthesis, characterization, and comparison of bactericidal and cytotoxic effects. *JEIM* **2013**, *227*, 1224−1236.

(61) Kamiloglu, S.; Sari, G.; Ozdal, T.; Capanoglu, E. Guidelines for cell viability assays. *Food Front.* **2020**, *1*, 332−349.

(62) Wang, H.; Li, Y.; Zuo, Y.; Li, J.; Ma, S.; Cheng, L. Biocompatibility and osteogenesis of biomimetic nano-hydroxyapatite/polyamide composite scaffolds for bone tissue engineering. *Biomaterials* **2007**, *28*, 3338−3348.

(63) Chaki, S. H.; Malek, T. J.; Chaudhary, M. D.; Tailor, J. P.; Deshpande, M. P. Magnetite Fe_3O_4 nanoparticles synthesis by wet

chemical reduction and their characterization. *Adv. Nat. Sci.: Nanosci. Nanotechnol.* **2015**, *6*, 035009.

(64) Kandamachira, A.; Selvam, S.; Marimuthu, N.; Janardhanan Kalarical, S.; Fathima Nishter, N. Collagen-nanoparticle Interactions: Type I Collagen Stabilization Using Functionalized Nanoparticles. *Soft Mater.* **2015**, *13*, 59−65.

(65) Gaidau, C.; Petica, A.; Micutz, M.; Danciu, M.; Vladkova, T. Progresses in treatment of collagen and keratin-based materials with silver nanoparticles. *Cent. Eur. J. Chem.* **2013**, *11*, 901−911.

(66) Eken, A. E.; Ozenbas, M. Characterization of nanostructured magnetite thin films produced by sol−gel processing. *J. Sol-Gel Sci. Technol.* **2009**, *50*, 321−327.

(67) Silva, V. A. J.; Andrade, P. L.; Silva, M. P. C.; Bustamante D, A.; De Los Santos Valladares, L.; Albino Aguiar, J. Synthesis and characterization of Fe_3O_4 nanoparticles coated with fucan polysaccharides. *J. Magn. Magn. Mater.* **2013**, *343*, 138−143.

(68) Tseng, T.; Hsieh, F.; Hsu, S. Increased cell survival of cells exposed to superparamagnetic iron oxide nanoparticles through biomaterial substrate-induced autophagy. *Biomater. Sci.* **2016**, *4*, 670−677.

(69) Peng, N.; Wu, B.; Wang, L.; He, W.; Ai, Z.; Zhang, X.; Wang, Y.; Fan, L.; Ye, Q. High drug loading and pH-responsive targeted nanocarriers from alginate-modified SPIONs for anti-tumor chemotherapy. *Biomater. Sci.* **2016**, *4*, 1802−1813.

(70) Chandra, S.; Barick, K. C.; Bahadur, D. Oxide and hybrid nanostructures for therapeutic applications. *Adv. Drug Delivery Rev.* **2011**, *63*, 1267−1281.

(71) Puett, D. DTA and heals of hydration of some polypeptides. *Biopolymers* **1967**, *5*, 327−330.

(72) Yamaura, M.; Camilo, R. L.; Sampaio, L. C.; Macedo, M. A.; Nakamura, M.; Toma, H. E. Preparation and characterization of (3-aminopropyl)triethoxysilane-coated magnetite nanoparticles. *J. Magn. Magn. Mater.* **2004**, *279*, 210−217.

(73) De Palma, R.; Peeters, S.; Van Bael, M. J.; Van den Rul, H.; Bonroy, K.; Laureyn, W.; Mullens, J.; Borghs, G.; Maes, G. Silane Ligand Exchange to make hydrophobic superparamagnetic nanoparticles water-dispersible. *Chem. Mater.* **2007**, *19*, 1821−1831.

(74) Zhang, Y.; Kohler, N.; Zhang, M. Q. Surface modification of superparamagnetic magnetite nanoparticles and their intracellular uptake. *Biomaterials* **2002**, *23*, 1553−1561.

(75) George, A.; Veis, A. FTIRS in water demonstrates that collagen monomers undergo a conformational transition prior to thermal self-assembly in vitro. *Biochem* **1991**, *30*, 2372−2377.

(76) de Campos Vidal, B.; Mello, M. L. S. Collagen type I amide I band infrared spectroscopy. *Micron* **2011**, *42*, 283−289.

(77) Li, H.; Luo, L.; Kunal, P.; Bonifacio, C. S.; Duan, Z.; Yang, J. C.; Humphrey, S. M.; Crooks, R. M.; Henkelman, G. Oxygen Reduction Reaction on Classically Immiscible Bimetallics: A Case Study of RhAu. *J. Phys. Chem. C* **2018**, *122*, 2712−2716.

(78) Villa, S.; Riani, P.; Locardi, F.; Canepa, F. Functionalization of Fe_3O_4 NPs by silanization: use of amine (APTES) and thiol (MPTMS) silanes and their physical characterization. *Materials* **2016**, *9*, 826.

(79) Geetha, B.; Mandal, A. B. The shape, size, aggregation, hydration, correlation times, and thermodynamic studies on macro monomer micelles. *J. Chem. Phys.* **1996**, *105*, 9649−9656.

(80) Rose, C.; Mandal, A. B. The interaction of sodium dodecyl sulfate and urea with cat-fish collagen solutions in acetate buffer: hydrodynamic and thermodynamic studies. *Int. J. Biol. Macromol.* **1996**, *18*, 41−53.

(81) Mandal, A. B.; Jayakumar, R. Aggregation, hydrogen bonding and thermodynamic studies on tetrapeptide micelles. *J. Chem. Soc., Faraday Trans.* **1994**, *90*, 161−165.

(82) Jayakumar, R.; Mandal, A. B.; Manoharan, P. T. Micelle formation of Boc-Val-Val-Ile-OMe tripeptide in chloroform and its conformational analysis. *J. Chem. Soc., Chem. Commun.* **1993**, *10*, 853−855.

(83) Jayakumar, R.; Jeevan, R. G.; Mandal, A. B.; Manoharan, P. T. Aggregation, hydrogen bonding and thermodynamic studies on Boc-Val-Val-Ile-OMe tripeptide micelles in chloroform. *J. Chem. Soc., Faraday Trans.* **1994**, *90*, 2725−2730.

(84) Mitra, T.; Sailakshmi, G.; Gnanamani, A.; Mandal, A. B. Dicarboxylic acid cross-linking interactions improves thermal stability and mechanical strength of reconstituted type I collagen. Part I. Oxalic acid. *J. Therm. Anal. Calorim.* **2011**, *105*, 325−330.

(85) Wang, Z.; Zhao, H.; Fan, L.; Lin, J.; Zhuang, P.; Yuan, W. Z.; Hu, Q.; Sun, J. Z.; Tang, B. Z.; Tang, Z. Chitosan rods reinforced by aligned multiwalled carbon nanotubes via magnetic-field-assistant in-situ precipitation. *Carbohydr. Polym.* **2011**, *84*, 1126−1132.

(86) Agnihotri, S.; Mukherji, S.; Mukherji, S. Immobilized silver nanoparticles enhance contact killing and show highest efficacy: elucidation of the mechanism of bactericidal action of silver. *Nanoscale* **2013**, *5*, 7328.

(87) Coelho, N. M.; Salmerón-Sánchez, M.; Altankov, G. Fibroblasts remodeling of type IV collagen at a biomaterials interface. *Biomater. Sci.* **2013**, *1*, 494.